J Solid State Electrochem (2005) 9: 882–889
DOI 10.1007/s10008-005-0040-8

ORIGINAL PAPER

Enn Lust · Priit Möller · Indrek Kivi · Gunnar Nurk
Silvar Kallip

Electrochemical characteristics of $La_{0.6}Sr_{0.4}CoO_{3-\delta}$, $Pr_{0.6}Sr_{0.4}CoO_{3-\delta}$ and $Gd_{0.6}Sr_{0.4}CoO_{3-\delta}$ on $Ce_{0.85}Sm_{0.15}O_{1.925}$ electrolyte

Received: 2 May 2005 / Revised: 19 May 2005 / Accepted: 15 June 2005 / Published online: 30 July 2005
© Springer-Verlag 2005

Abstract Cyclic voltammetry, chronoamperometry and electro-chemical impedance have been used for the analysis of the following medium temperature half-cells: $Ce_{0.85}Sm_{0.15}O_{1.925}$| $La_{0.6}Sr_{0.4}CoO_{3-\delta}$, $Ce_{0.85}Sm_{0.15}O_{1.925}$| $Pr_{0.6}Sr_{0.4}CoO_{3-\delta}$ and $Ce_{0.85}Sm_{0.15}O_{1.925}$| $Gd_{0.6}Sr_{0.4}CoO_{3-\delta}$. The influence of the atomic mass of the A–site cation in the perovskite cathode on the oxygen reduction kinetics has been discussed. The total polarisation resistance, obtained from the Z'', Z'-plots, increases with the rise of atomic mass of the cation in the A-site position. Two different time constants have been obtained for the oxygen electroreduction process, and the replacement of La^{3+} by Gd^{3+} in the cathode material decreases somewhat the surface catalytic activity, but the noticeably higher low-frequency series resistance, i.e. mainly diffusion-like mass transfer resistance, values have been obtained. However, the mainly diffusion-limited process at $T \leq 773$ K for $Gd_{0.6}Sr_{0.4}CoO_{3-\delta}$ and the kinetically mixed process (diffusion + charge transfer) for $Pr_{0.6}Sr_{0.4}CoO_{3-\delta}$ and $La_{0.6}Sr_{0.4}CoO_{3-\delta}$ have been established. At higher temperature ($T \geq 993$ K) and more negative potentials, the O_2 reduction process is limited mainly by the heterogeneous charge transfer step.

Keywords Solid oxide fuel cell $Ce_{0.85}Sm_{0.15}O_{1.95}$ electrolyte · $La_{0.6}Sr_{0.4}CoO_{3-\delta}$ · $Pr_{0.6}Sr_{0.4}CoO_{3-\delta}$ · $Gd_{0.6}Sr_{0.4}CoO_{3-\delta}$ · Cathode

Presented at the fourth Baltic Conference on Electrochemistry, Greifswald, March 13–16, 2005.

E. Lust (✉) · P. Möller · I. Kivi · G. Nurk · S. Kallip
Institute of Physical Chemisty, Tartu University,
2 Jakobi Street, 2400, Tartu, Estonia
E-mail: enn.lust@ut.ee
Tel.: +37-27-375165
Fax: +37-27-375160

Introduction

In our previous works [1–5], the electroreduction kinetics of O_2 at various cathode|electrolyte interfaces, including $La_{0.6}Sr_{0.4}CoO_{3-\delta}$, $La_{0.6}Sr_{0.4}Co_{1-y}Fe_yO_{3-\delta}$ and 70 wt% $La_{0.6}Sr_{0.4}CoO_{3-\delta}$ + 30 wt% $Ce_{0.8}Gd_{0.2}O_{1.9}$ mixed cathodes, has been studied. The mixed cobaltite–electrolyte cathode sintered at $T < 1{,}323$ K did not have so high catalytic activity as the pure porous $La_{1-x}Sr_xCoO_{3-\delta}$ cathode. Comparison of the data for $Ce_{0.8}Gd_{0.2}O_{1.9}$| $La_{0.6}Sr_{0.4}CoO_{3-\delta}$ (CGO|LSCO) and $Ce_{0.8}Sm_{0.2}O_{1.9}$| $La_{0.6}Sr_{0.4}CoO_{3-\delta}$ (CSO|LSCO) half-cells demonstrate a higher O_2 reduction activity for CSO|LSCO than for CGO|LSCO half-cell [1] and therefore the more detailed studies at CSO|cathode interface are reasonable. The influence of the chemical nature of the atoms positioned into the perovskite A-site and substitution of the A-site cations with cations in the 2+ oxidation state (activation) as well as the microstructure of the cathode and anode are the open questions [1–35].

The very good ionic and electronic conductivities have been obtained for $Pr_{1-x}Sr_xCoO_{3-\delta}$ (PSCO) and $Gd_{1-x}Sr_xCoO_{3-\delta}$ (GSCO) perovskites [15, 24–27]; however, there are no systematic experimental data obtained under cathodic polarisation during long operation times as well as under conditions of repetitive thermocycling. The maximum electrical conductivity ρ for PSCO has been obtained at $x = 0.4$ and introduction of the Sr^{2+} cations into the A-site of the orthorhombic perovskite lattice is compensated by oxidation of Co^{3+} to Co^{4+} (holes) at $x \leq 0.15$ and by the formation of the oxygen vacancies even at room temperature when $x \geq 0.4$ [24, 25]. According to Rossignol et al. [24] $Pr_{0.5}Sr_{0.5}CoO_{3-\delta}$ and $Gd_{0.5}Sr_{0.5}CoO_{3-\delta}$ show the best performance on the $Ce_{1-x}Gd_xO_{2-\delta}$ electrolyte, achieving an area-specific resistance (ASR) between 0.1 and 0.2 Ω cm^2 at 923 K. At $T < 923$ K, the values of ASR were very high [24].

The main aim of this work was to synthesise $Pr_{0.6}Sr_{0.4}CoO_{3-\delta}$ (PSCO) and $Gd_{0.6}Sr_{0.4}CoO_{3-\delta}$ (GSCO)

cathode materials and to prepare the $Ce_{0.85}Sm_{0.15}O_{1.925}|La_{0.6}Sr_{0.4}CoO_{3-\delta}$ (Sys1), $Ce_{0.85}Sm_{0.15}O_{1.925}|Pr_{0.6}Sr_{0.4}CoO_{3-\delta}$ (Sys2) and $Ce_{0.85}Sm_{0.15}O_{1.925}|Gd_{0.6}Sr_{0.4}CoO_{3-\delta}$ (Sys3) half-cells and to investigate the electrochemical characteristics of these half-cells at the same experimental working conditions.

Experimental

Preparation of cathode materials and electrolytes

Commercially available powders of La_2O_3 (99.99%), Pr_6O_{11} (99.99%), Gd_2O_3(99.9%), $SrCO_3$ (99.9%) and Co_3O_4 (99.9%) have been used for the synthesis of the LSCO, PSCO and GSCO powders, using the conventional solid-state reaction technique [1–5, 8, 15, 20, 25–27]. Powders with the stoichiometric compositions were ball-milled in a zirconia mill container with zirconia grinding balls in H_2O for 8 h and after drying calcined at 1,473 K for 10 h to form a perovskite phase. The perovskite (trigonal R-3c at $T = 293$ K) phase was crushed and ball-milled for 3 h using the same system [1]. The X-ray diffraction (XRD) measurements indicate the formation of the single-phase perovskite structure for LSCO and PSCO. In agreement with the data of works [20–24], it was established that the solubility of Sr^{2+} ions in the lattice of $GdCoO_{3-\delta}$ is lower than in $LaCoO_{3-\delta}$ or $PrCoO_{3-\delta}$, and the doping levels higher than 25% lead to the segregation of second perovskite-like phase and therefore $Gd_{0.6}Sr_{0.4}CoO_{3-\delta}$ is not a single-phase cathode material. The CSO electrolyte was prepared from the corresponding oxides CeO_2 (99.9%) and Sm_2O_3 (99.99%), using conventional solid-state reaction technique discussed in detail in our previous papers [1–5, 28].

The cathode material synthesised and characterised was mixed with an appropriate amount of organic binder (ethyl cellulose) and solvent (turpentine oil) and screen-printed on one side of the CGO electrolyte. The working electrodes with surface area $S_{el} = 0.5$ cm^2 were fired at 1,323 K in air for 8 h and characterised by XRD and SEM methods before application of the counter and reference electrodes. A three-electrode assembly used was analogous to that discussed in [1–5, 8]. The ac frequency f was changed from 10 MHz to 0.01 Hz and the ac voltage amplitude was 5 mV. The ohmic series resistance R_{ex} of the system (bulk electrolyte + contact and Pt wire resistances) was determined from the impedance data at very high frequency $f \geq 5\times10^5$ Hz ($Z(\omega \rightarrow \infty) = R_{ex}$; $\omega = 2\pi f$) at $E = 0$ V (vs. Pt|porous Pt|O_2 reference electrode). The voltage range applied between working and counter electrodes was not over 3...5 V for the extreme polarisations $E = -1.0$ V and at lower temperature $T \leq 773$ K used in this work. The very good cyclability of the current density j versus potential curves and a very small hysteresis between the cathodic and anodic potential scans (discussed later) indicate that the degradation of the electrolyte under cathodic polarisation is negligible. The very high frequency series resistance, independent of the cathodic potential applied, indicates the high stability of the electrolyte and absence of electron migration effect in the cathode material.

The electrode materials have been characterised using XRD, SEM, gas adsorption (BET) (Fig. 1) and AFM (Fig. 2) methods. Special big samples from the cathode, prepared under the same experimental conditions as the cathodes, have been used for the BET analysis. These cathode materials are porous with specific surface areas S_{BET} 6.0, 6.5 and 10.5 m^2 g^{-1} for PSCO (Sys2), GSCO (Sys3) and LSCO (Sys 1), accordingly, and there are transport pores ($d < 1\times10^{-6}$ m) (in good agreement with the electronmicroscopy data) as well as meso and submicro pores with the mean diameter of $d \sim 1.8$ nm (Fig. 2) inside the cathode material. The size of the particles varies from 0.5 to 2.5 μm, and surface roughness factor R equal to 1.45 and root mean square height of the cathode surface R_{ms} equal to 334 nm have been obtained from the AFM data (Fig. 2).

Before cyclic voltammetry and impedance measurements, the chronoamperometry curves have been measured (discussed later). After current stabilisation (10–30 s) followed by the potential step, the Z'', Z' plots at fixed potential have been measured.

Results and discussion

Experimental complex plane (Nyquist and Bode) plots

Figures 3 and 4 show some selected complex impedance plane (Z'', Z'-) plots (so-called Nyquist plots) for Sys 2 and Sys 3, measured at different temperatures ($773 \leq T \leq 973$ K) and electrode potentials E (vs. Pt|porous Pt|O_2), where $Z'' = (j\omega\, C_s)^{-1}$ is the imaginary part and Z' is the real part of the complex impedance Z. The Z'', Z'- plots

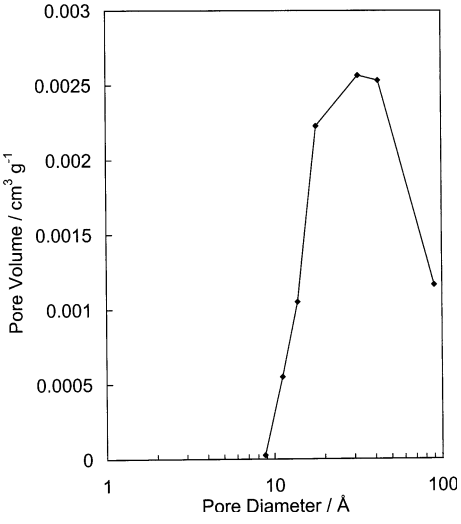

Fig. 1 Incremental pore volume versus pore diameter plot for the $La_{0.6}Sr_{0.4}CoO_{3-\delta}$ cathode ($S_{BET} = 10.5$ m g^{-1})

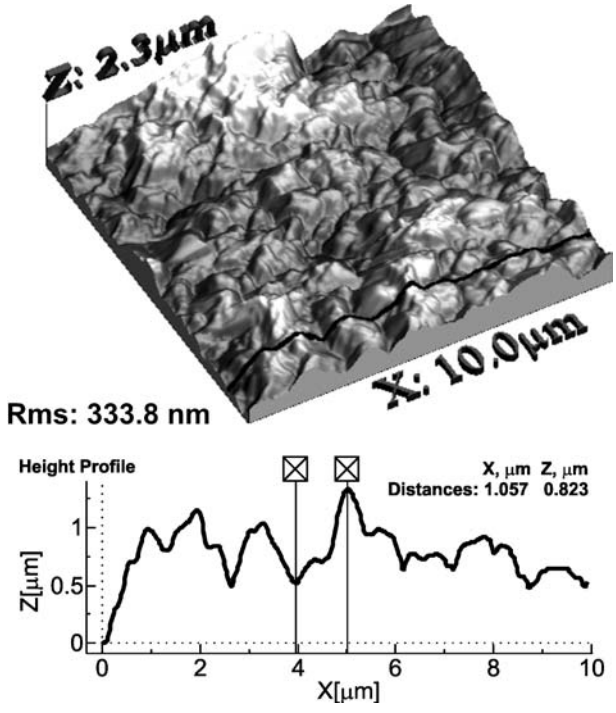

Fig. 2 AFM images of microstructure, height profiles and the value of the root mean square height (R_{ms}) for the $Gd_{0.6}Sr_{0.4}CoO_{3-\delta}$ cathode

display a capacitive behaviour at ac f from 0.1 MHz to 0.01 Hz. In the region of f from 0.5 MHz to 5 kHz a very well separable semicircle has been found for Sys1 and Sys2, corresponding to the conductivity process in the bulk electrolyte (at $f > 100$ kHz) as well as to the O^{2-} ion transport at the cathode| electrolyte phase boundary (5 kHz $< f <$ 100 kHz) [1–5, 11, 12, 31, 32]. Comparison of the data for half-cells with $Ce_{0.85}Sm_{0.15}O_{1.925}$ and $Ce_{0.8}Gd_{0.2}O_{1.9}$ electrolytes [1–5] shows that the high-frequency part of the Z'', Z'-plots is mainly influenced by the electrolyte|cathode phase boundary

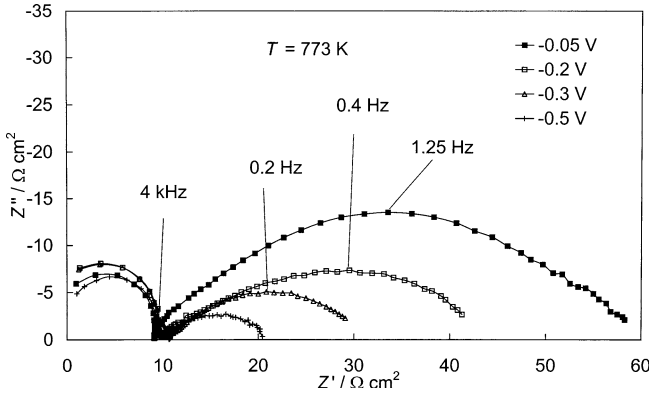

Fig. 3 Nyquist (Z'', Z') plots for $Pr_{0.6}Sr_{0.4}CoO_{3-\delta}$| $Ce_{0.85}Sm_{0.15}O_{1.925}$ half-cell at 773 K and at electrode potentials (noted in figure) versus Pt| porous Pt| O_2 reference electrode. (*Solid lines* fitting according to the circuit in Fig. 5b)

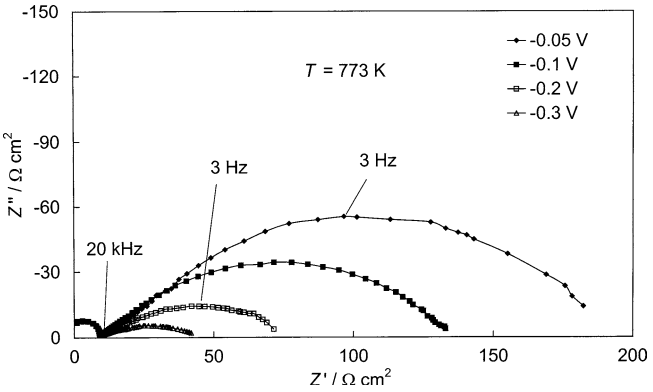

Fig. 4 Nyquist plots for $Gd_{0.6}Sr_{0.4}CoO_{3-\delta}$| $Ce_{0.85}Sm_{0.15}O_{1.925}$ half-cell at $T = 773$ K and at electrode potentials, noted in figure. (*Solid lines* fitting according to the circuit in Fig. 5b)

characteristics [1–5, 8]; the lower specific conductivity σ_{ex} for CGO electrolyte in comparison with CSO has been calculated. The values of R_{ex} for LSCO|CSO interface are lower than those for GSCO|CSO interface, which is probably caused by the non-single-phase structure of GSCO. The values of R_{ex} are independent of the cathodic potential applied (from 0 to −1.0 V) as well as of the sequence of measurements of the Z'', Z'-plots. There is no change in R_{ex} compared before and after recording the cyclic voltammetry and Nyquist plots. Thus, under the experimental conditions used in this work there is no remarkable degradation, i.e. reduction of the electrolyte and generation of electronic charge carriers into the electrolyte.

In the region from 5 kHz to 0.01 Hz, at least two arcs (Figs. 3, 4), characterised with two time constants ($\tau = (2\pi f_{max})^{-1}$ where f_{max} is the frequency of the maximum in the Z'', Z'-plot), were observed at lower temperatures ($T < 873$ K). The medium-frequency arc 1 for LSCO and GSCO is noticeably smaller (Fig. 4) but for PSCO| CSO the medium frequency arc is wider than the low-frequency arc 2 (Figs. 3, 4). The width of the arc1, corresponding to the polarisation resistance of the medium-frequency process ($R_{p,m}$), decreases with T, and the time constant τ_1 decreases with increasing T and describes the ionisation of adsorbed O_{ads} at the outer (more open) cathode surface with interfacial adsorption/absorption capacitance C_1 [1, 2]. $R_{p,m}$ depends on the cathode potential, and the characteristic time constant τ_1 for the arc 1 somewhat increases with the cathodic polarisation (Fig. 4). Thus, the reaction zone moves from the more open area toward the nanopores inside the cathode with increasing the negative polarisation. The total polarisation resistance $R_{p,t}$ increases in the order Sys1 < Sys2 < Sys3 at $T = 973$ K. $R_{p,t}$ decreases with the rise of temperature and negative electrode potential. The same dependence is valid at given E with increasing T. With increasing T over 973 K and at higher negative potentials the arc 1 for Sys 1 disappears.

The low-frequency arc 2 becomes more depressed with increasing T and $|E|$, which can be explained by the

less pronounced adsorption and diffusion (i.e. mass transfer) limited behaviour at higher temperatures and negative potentials. Time constant for the arc 2 (τ_2) is independent of the electrolyte composition at fixed T and E [1–5] but depends on the specific surface area of the cathode (chemical composition of the cathode). τ_2 noticeably decreases with the increase of T at fixed E, and with the negative polarisation at fixed T.

The decrease in phase angle $|\delta|$ with increasing temperature and negative electrode potential indicates that the "true" charge transfer process is the rate-determining step at $f < 10$ Hz ($\delta \approx -2°$ at $T \geq 973$ K and at $E \leq -0.2$ V). The different absolute values of the relaxation frequency f_{max} and dependences of $|\delta|$ on $\log f$ for Sys1, Sys 2 and Sys 3 indicate that the characteristic relaxation time for the low-frequency process decreases with increasing molar volume of the A-site cation, i.e. with the specific surface area of the cathode.

Fitting of the Nyquist plots

The data in Figs.3 and 4, to a first approximation, can be fitted by the equivalent circuit (solid lines—fitting, points—experimental), presented in Fig. 5 and discussed in our works [1–5]. The elements R_{gb} and C_{gb} in Fig. 5 characterise the grain boundary processes at the cathode| electrolyte interface and, in comparison with LSCO|CSO, the influence of R_{gb} and C_{gb} on the characteristics of the PSCO|CSO and GSCO|CSO interfaces is not very well detectable. It is mainly caused by the noticeably higher interface area between porous LSCO cathode and electrolyte [1].

The medium as well as low-frequency arcs can be fitted by the constant phase element CPE_1 and CPE_2 (with Z_{CPE} equal to $A^{-1}(j\omega)^{-\alpha}$, where A is constant and α is the fractional exponent) and charge transfer resistances R_1 and R_2 connected in parallel, respectively (circuit in Fig. 5a) (if $\alpha = 1$ then A is equal to the electrical double layer capacitance C_{dl}). The fractional exponent $\alpha_1 > 0.5$ and very low values of R_1 for arc 1 (Fig. 6a) indicate that the diffusion-like mass transfer limited so-called "true" charge transfer process is the rate-determining step at $f > 10$ Hz and $T < 823$ K [36–42]. The values of C_1 (Fig. 6b) increase with increasing T and E, thus the accumulation of partially reduced oxygen species into the cathode material takes place [1–5, 36–42]. R_1 has a maximum at small negative potentials (Fig. 6a) and is higher for GSCO cathodes than for PSCO and LSCO. For LSCO, there is a very weak dependence of R_1 on E, but the values of R_1 decrease exponentially with increasing temperature.

The values of α_2 nearly equal to 0.5 for the arc 2 indicate that CPE_2 behaves as a Warburg- type diffusional impedance Z_W,2. Thus, the CPE_2 can be exchanged with the generalised finite Warburg element (GFW) for a short circuit terminus model [41, 42] (circuit in Fig. 5b) expressed as

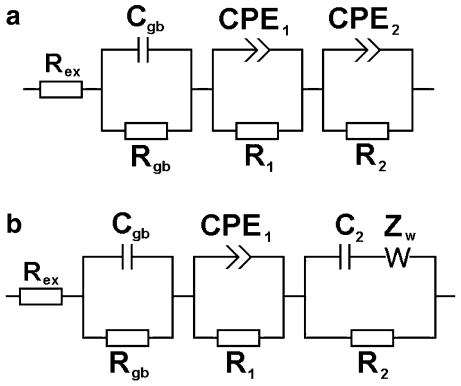

Fig. 5 Equivalent circuits used for fitting the complex impedance plane plots (**a**). R_{ex} is the high-frequency series resistance ($R_{ex} \rightarrow Z'$ if $\omega \rightarrow \infty$); C_{gb} and R_{gb} are the grain boundary capacitance and resistance, respectively; CPE_1, C_1 and R_1 are the high-frequency constant phase element, capacitance and resistance, respectively; CPE_2, C_2 and R_2 are the low-frequency constant phase element, capacitance and resistance, respectively; Z_W is the Warburg-like diffusion impedance

$$Z_{GFW} = \frac{R_D \tanh\left(jL^2\omega/D\right)^{\alpha_W}}{\left(jL^2\omega/D\right)^{\alpha_W}}, \quad (1)$$

where R_D is the limiting diffusion resistance, L and D the effective diffusion layer thickness and effective diffusion

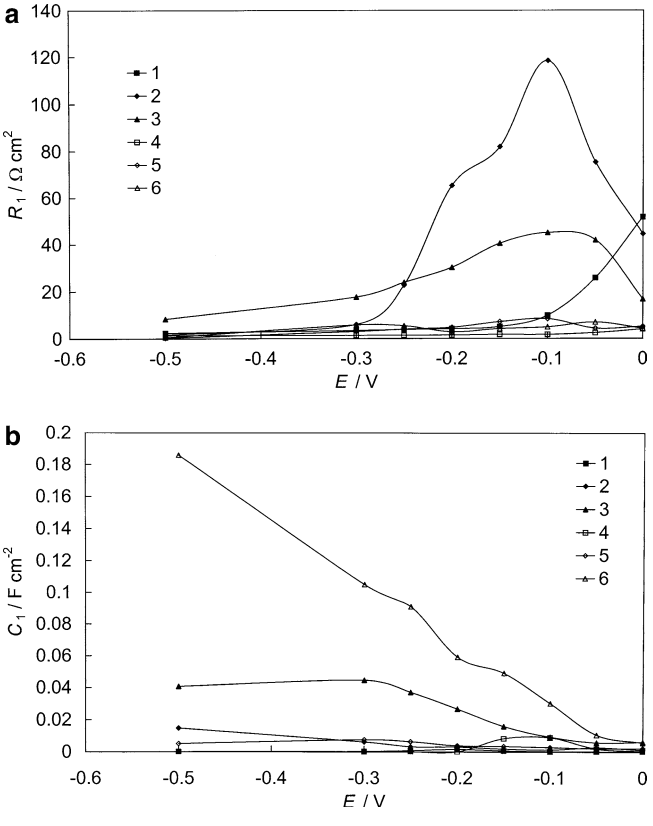

Fig. 6 Medium frequency resistance (**a**) and capacitance (**b**) versus E plots for $La_{0.6}Sr_{0.4}CoO_{3-\delta}$ (1; 4), $Gd_{0.6}Sr_{0.4}CoO_{3-\delta}$ (2; 5) and $Pr_{0.6}Sr_{0.4}CoO_{3-\delta}$ (3; 6) cathodes on the $Ce_{0.85}Sm_{0.15}O_{1.925}$ electrolyte at $T = 773$ K (1–3) and $T = 873$ K(4–6)

coefficient, respectively, and α_w a fractional exponent in Z_{GFW} [36–42].

The very small chi-square function values $\chi^2 < 2\times10^{-4}$, relative residuals Z_{res}' and Z_{res}' [36, 37] and weighted sum of squares $\Delta^2 < 0.020$ for PSCO and LSCO have been calculated, using the equivalent circuit presented in Fig. 5b. Attempts to use the equivalent circuit, where the Gerischer impedance was added into the parallel circuit [12], did not give satisfactory fitting results (error in the Gerischer impedance resistance was very high) and therefore these data will not be discussed in more detail in this article. Thus, the surface exchange process seems not to be a rate-determining step for LSCO, PSCO and GSCO.

According to the results of fitting, the arc 2 at lower T and negative potentials characterises the kinetically mixed, charge transfer (with corresponding resistance R_2, Fig. 7a) and diffusion-like limited oxygen reduction processes. The diffusion resistance R_D (Fig. 7b) and R_2 (Fig. 7a) at $T < 873$ K decrease nearly exponentially with rising negative potential, which can be explained by the charge transfer process with the Arrhenius-like activation mechanism. The dependences of R_D and so-called frequency factor T (Fig. 7c) on E indicate the very complicated mass transfer process as the resistance of the semi-infinite Fick-like diffusion process has to be independent of E. The increase in α_W with increasing T indicates the deviation of the system from the adsorption-limited anomalous diffusion model [41–43] toward the semi-infinite diffusion model ($\alpha_W = 0.5$) [37–40] with the decrease of the electroreduction process rate. The decrease in the low-frequency capacitance C_2 with E is in good agreement with this conclusion. It should be noted that the surface diffusion, Knudsen-like and finite-length diffusion as well as migration of charged oxygen species are possible mass transfer mechanisms inside the porous cathode [1–5, 43–45]. The low-frequency capacitance C_2 (i.e. adsorption, absorption or pseudocapacitance, caused by the charge transfer process of reduction) increases with rising temperature at moderate E. At fixed temperature and $E > -0.15$ V the values of R_D are noticeably higher than R_2, indicating the mainly mass transfer limited reaction mechanism. The values of R_D and R_2 increase with the atom mass of the A-site cation, i.e. with decreasing specific surface area of the cathode.

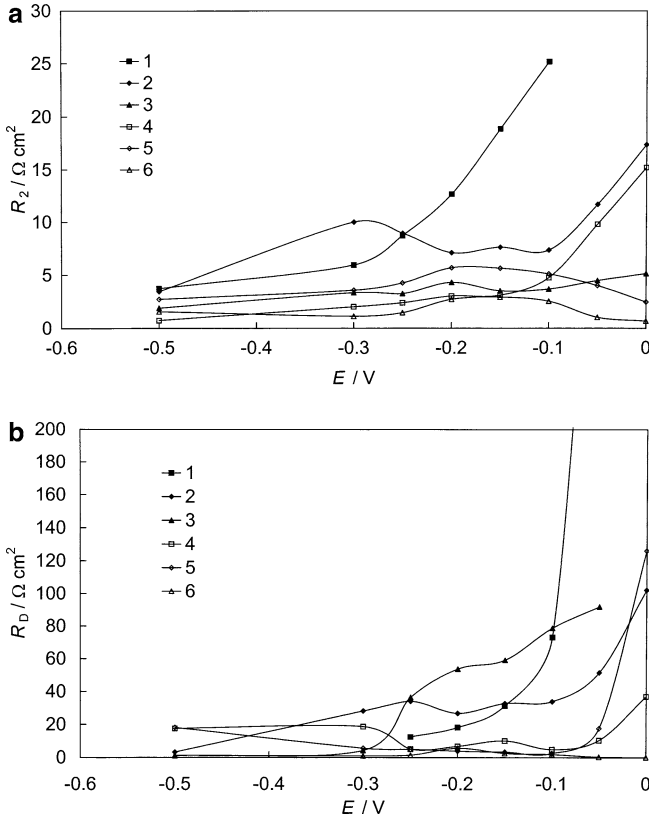

Fig. 7 Low-frequency charge transfer resistance R_2 (**a**) and diffusion resistance R_D (**b**) versus electrode potential dependences for $La_{0.6}Sr_{0.4}CoO_{3-\delta}$ (1; 4), $Gd_{0.6}Sr_{0.4}CoO_{3-\delta}$ (2; 5) and $Pr_{0.6}Sr_{0.4}CoO_{3-\delta}$ (3; 6) cathodes on the $Ce_{0.85}Sm_{0.15}O_{1.925}$ electrolyte at $T = 773$ K (1–3) and $T = 873$ K(4–6). (Fitting according to circuit in Fig. 5b)

Activation energy and Tafel-like overpotential versus current density plots

The capacitive parts of the Z'', Z'-plots (at $f < 10$ kHz) were used to determine the total polarisation resistance of oxygen reduction R_p (taking into account the ohmic and activation polarisations, as well as the mass transport limitation characteristics of the oxygen reduction process) from the difference between the intercepts of the very low and high frequency parts of the spectra with the Z'-axis of Nyquist plots. Including the arc 1 and arc 2, the cathode polarisation resistance R_p is less than 0.9, 1.2 and 1.3 Ω cm^2 at $T = 973$ K for Sys1, Sys2 and Sys 3, respectively. Somewhat higher R_p values have been obtained for LSCO, PSCO and GSCOin the case of CGO electrolyte at the same temperatures [1, 2]. On the other hand, the fitting data can be used for obtaining the polarisation resistance values for the medium-frequency process (arc 1), $R_{p,m}$, and low-frequency process, $R_{p,l}$, at fixed E. R_p, $R_{p,m}$ and $R_{p,l}$ have been used for the calculation of the cathode reaction conductivity σ_t, σ_1 and σ_2 values. The nearly linear dependences of $\log\sigma_t$, $\log\sigma_1$ and $\log\sigma_2$ on $(T)^{-1}$ at fixed E have been used for the calculation of the values of activation energy (Fig. 8). At $E = -0.1$ V, the values of activation energy for total reduction process, A_t, have been obtained as 0.75; 0.6 and 0.57 eV for Sys1, Sys2 and Sys3, respectively, decreasing very slightly with the increase of the negative potential of the cathode.

The dependences of current density (j) on potential (Fig. 9a) and time (t) (chronoamperometry data, Fig. 9b), when the cathode was stepped to the potentials $E = -0.1$ and -0.25 V with respect to a Pt| porous Pt| O_2 reference electrode, indicate that the shape of the j, t-curves depends on T and E as well as on the cathode material studied. The missing hysteresis in the cyclic voltammograms (Fig. 9a) indicates that there are no irreversible processes in the cathode as well as in the

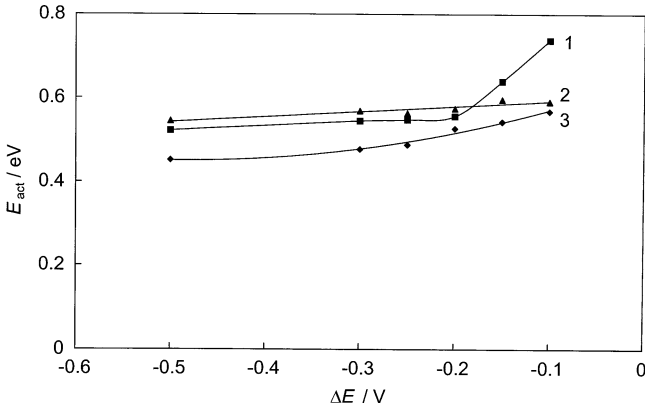

Fig. 8 Total activation energy versus electrode potential plots for $La_{0.6}Sr_{0.4}CoO_{3-\delta}$ (1), $Gd_{0.6}Sr_{0.4}CoO_{3-\delta}$ (2) and $Pr_{0.6}Sr_{0.4}CoO_{3-\delta}$ (3) cathodes on the $Ce_{0.85}Sm_{0.15}O_{1.925}$ electrolyte

electrolyte material at high negative electrode potentials (overpotentials) applied at low temperature. It should be noted that there are only very small changes in the shape of cyclic *j, E* curves obtained during tenth to hundred cycles of potential. According to Fig. 9b, the value of *j* increases at the first moment after potential step and thereafter decreases with time at very short times ($t < 3$ s) but *j* is practically independent of time at $t \geq 3$ s. The decrease in *j* at short times can be explained by the not very low diffusion resistance (by slow diffusion of the partially reduced oxygen species) for the composite cathode material and by the measurable reduction overpotential of the system. The independence of *j* at longer times can be explained by the stabilisation of the O_2 reduction layer thickness inside the porous cathode material. At higher *T* the stable current density values have been established at more short times. Thus, at lower *T* and *E*, the oxygen reduction is probably limited by the mass transfer step of the oxygen species to the reaction zone and the interface reaction (at open outer surface) does not contribute significantly to the overall reaction. At higher *T* and $|E|$, the reaction is probably less controlled by the rate of the mass transfer of the partially reduced oxygen species. The increase in the concentration of the oxygen vacancies with increasingly negative potential will improve the mass transfer of the "charged species", leading to the increase of catalytic activity [1–5, 8].

These results are in good agreement with the values of the transfer coefficient, obtained from the Tafel-like η,log *j*-curves (Fig. 10), which are linear if $|\eta| < 0.4$ V [1–5]. At higher values of $|\eta|$, the small deviation of log *j*,η-plots from linearity has been established, which is caused by the rise of the electronic conductivity of the CSO electrolyte. Taking into account the probable irreversible nature of this process, these extreme cathodic potentials have not been studied systematically in this work. The values of $\alpha_c > 0.5$ have been established for Sys 1, Sys 2 and Sys 3 at lower temperature (if the number of electrons transferred at the limiting step, *n*, has been taken equal to 1). Thus, the O^-_{ads} diffusion-like step seems to be the rate-determining step for the electroreduction reaction [1–5, 36–40, 44, 45] in good agreement with the impedance spectroscopy data. The values of the exchange current density j_0 [44, 45], obtained at fixed temperatures, decrease in the order PSCO > GSCO > LSCO (Fig. 11). j_0 increases with *T* and there is nearly linear dependence of $\ln j_0$ on *T*. The constant *a* in the Tafel equation ($\eta = a + b \log j$) depends on the

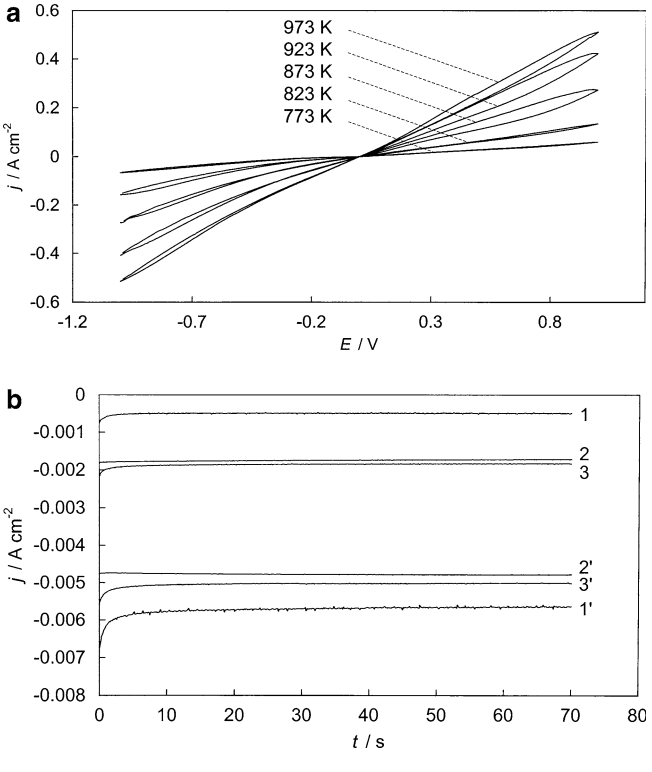

Fig. 9 Cyclic voltammetry curves (at temperatures given in figure) (**a**) and chronoamperometry data (**b**) for $La_{0.6}Sr_{0.4}CoO_{3-\delta}$ (1; 1′),$Gd_{0.6}Sr_{0.4}CoO_{3-\delta}$ (2; 2′) and $Pr_{0.6}Sr_{0.4}CoO_{3-\delta}$ (3; 3′) cathodes on the $Ce_{0.85}Sm_{0.15}O_{1.925}$ electrolyte at $T = 773$ K and potential steps Δ(*E*) −0.1 V (1–3) and −0.25 V (1′–3′)

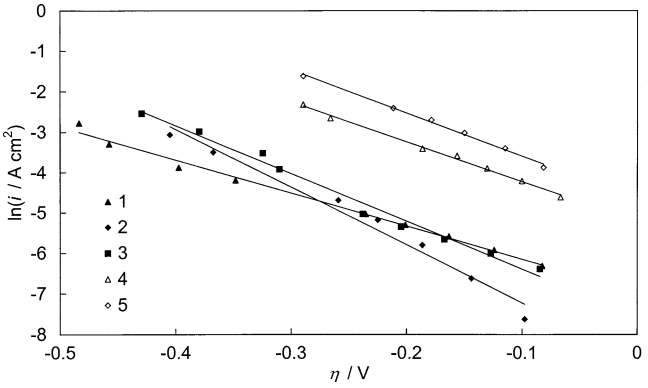

Fig. 10 Current density versus overpotential plots for $Pr_{0.6}Sr_{0.4}CoO_{3-\delta}$ (1; 4), $La_{0.6}Sr_{0.4}CoO_{3-\delta}$ (2; 5) and $Gd_{0.6}Sr_{0.4}CoO_{3-\delta}$ (3) cathodes on the $Ce_{0.85}Sm_{0.15}O_{1.925}$ electrolyte at $T = 773$ K (1–3) and $T = 873$ K (4,5)

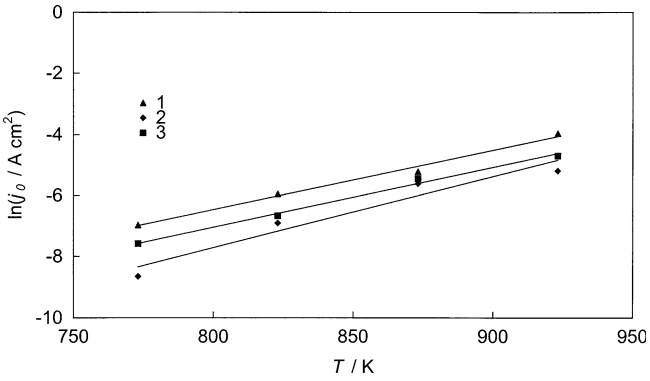

Fig. 11 Exchange current density versus temperature dependences (obtained from Fig. 10) for $Pr_{0.6}Sr_{0.4}CoO_{3-\delta}$ (1), $La_{0.6}Sr_{0.4}CoO_{3-\delta}$ (2) and $Gd_{0.6}Sr_{0.4}CoO_{3-\delta}$ (3) cathodes on the $Ce_{0.85}Sm_{0.15}O_{1.925}$ electrolyte

cathode nature and the absolute values of $|a|$ increase at given temperature in the order LSCO≤ GSCO ≤ PSCO.

Long-term stability has been tested at $T = 973$ K and $E = -0.3$ V during 1500 hours for Sys1. It should be noted that during the operation period at least 10 thermocycles have been made. The ac impedance measurements distinguished the electrolyte and cathode reaction resistance values practically independent of the operation time of the half-cell and thermocycle number. The results of fitting the Nyquist plots show that there are no big changes in the equivalent circuit parameters with time and these half-cells can be used for the future operation-time tests going on in our laboratory.

Conclusions

$Ce_{0.85}Sm_{0.15}O_{1.925}|\ La_{0.6}Sr_{0.4}CoO_{3-\delta}$, $Ce_{0.85}Sm_{0.15}O_{1.925}|\ Pr_{0.6}Sr_{0.4}CoO_{3-\delta}$ and $Ce_{0.85}Sm_{0.15}O_{1.925}|\ Gd_{0.6}Sr_{0.4}CoO_{3-\delta}$ half-cells have been studied using electro-chemical impedance, cyclic voltammetry and chronoamperometry methods. Detailed analysis of the complex impedance (Z'', Z') plots shows that the total polarisation resistance increases with the rise of the atomic mass of the cation in the A-site position and two different time constants have been obtained for the cathode process, i.e. for oxygen electroreduction. Various equivalent circuits have been used for fitting the Nyquist (Z'', Z'-) plots. A better fit has been established using a model, which was fitted by equivalent circuit taking into account the charge transfer process at grain boundaries (at high frequencies) and the medium and low-frequency O_2 electroreduction process at the cathode surface and inside the porous cathode material. The low-frequency series resistance and diffusion resistance increase in the order $La_{0.6}Sr_{0.4}CoO_{3-\delta} < Pr_{0.6}Sr_{0.4}CoO_{3-\delta} < Gd_{0.6}Sr_{0.4}CoO_{3-\delta}$ with decrease in the specific surface area. It was found that the replacement of La^{3+} by Gd^{3+} in the cathode material decreases somewhat the surface catalytic activity but noticeably higher low-frequency series resistance (i.e. mainly diffusion-like mass transfer resistance R_D) values have been obtained. It was found that the mainly diffusion-limited process at $T \leq 773$ K for $Gd_{0.6}Sr_{0.4}CoO_{3-\delta}$ deviates toward the kinetically mixed process (diffusion + charge transfer) with increasing temperature. At $T \geq 993$ K and more negative potentials, the O_2 reduction is limited mainly by the heterogeneous charge transfer step.

Acknowledgements This work is supported by ESF grant No. 6467 and by AS Elcogen under the grants LFKFE 01081 and LFKFE 03006.

References

1. Lust E, Nurk G, Kallip S, Kivi I, Möller P (2005) Electrochemical characteristics of $Ce_{0.8}Gd_{0.2}O_{1.9}|\ La_{0.6}Sr_{0.4}CoO_{3-\delta} + Ce_{0.8}Gd_{0.2}O_{1.9}$ half-cell. J Solid State Electrochem (in press)
2. Lust E, Nurk G, Kallip S, Kivi I, Möller P, Nigu P, Lust K, Influence of electrode polarisation on the characteristics of some medium temperature half-cells for SOFC. Electrochim Acta (in review)
3. Lust E, Nurk G, Kallip S, Kivi I, Möller P, Nigu P, Lust K (2004) Proceedings of 6th European fuel cell forum, Lucerne, p 1271
4. Lust E, Möller P, Kivi I, Nurk G, Kallip S, Nigu P, Lust K (2005) In: Proceedings of 9th international symposium on solid oxide fuel cells, Quebec (p. 1607)
5. Nurk G, Kallip S, Kivi I, Möller P, Lust E (2004) Proceedings of 6th European fuel cell forum, Lucerne, p 887
6. Singhal SC (2000) Solid State Ionics 135:305
7. Weber A, Ivers-Tiffée E (2004) J Power Sources 127:273
8. Nurk G, Kallip S, Kivi I, Möller P, Lust E (2004) Proceedings of 6th European fuel cell forum, Lucerne, p 887
9. Dusastre V, Kilner A (1999) Solid State Ionics 126:163
10. Jiang SP (2002) Solid State Ionics 146:1
11. Mogensen M, Sammes NM, Tompsett GA (2000) Solid State Ionics 129:63
12. Adler SB (1998) Solid State Ionics 111:125
13. Gödickemeier M, Gauckler LJ (1998) J Electrochem Soc 145:414
14. Tedmon CS, Spacil HS, Mitoff SP (1969) J Electrochem Soc 116:1170
15. Yamamoto O, Takeda Y, Kanno R, Noda M (1987) Solid State Ionics 22:241
16. Teraoka Y, Zhang H, Furukawa S, Yamazoe N (1985) Chem Lett 14:1743
17. Arai H, Yamada T, Egachi K, Seigama T (1986) Appl Catal 26:394
18. Esquirol A, Brandon NP, Kilner JA, Mogensen M (2004) J Electrochem Soc 151:1847
19. Eastabook JN (1957) Philos Mag (Eight Sek) 2:1421
20. Klostogloudis GCh, Vasilakos N, Ftikos Ch (1998) Solid State Ionics 106:207
21. Goodenough JB (1958) J Phys Chem Solids 6:287
22. Raccah PM, Goodenough JB (1967) Phys Rev 155:932
23. Bhide VG, Rajoria DS, Rama Rao G, Rao CNR (1972) Phys Rev B 6:1021
24. Ralph JM, Rossignol C, Kumar R (2003) J Electrochem Soc 150:1518
25. Rossignol C, Ralph JM, Bae JM, Vaughey JT (2004) Solid State Ionics 175:59
26. Takeda Y, Ueno H, Imanishi N, Yamamoto O, Sammes N, Phillips MB (1996) Solid State Ionics 86–88:1187
27. Phillips MB, Sammes NM, Yamamoto O (1999) Solid State Ionics 123:131
28. Kleitz M, Tetitbon F (1996) Solid State Ionics 92:65
29. Mantzavinos D, Hartley A, Metcalfe IS, Sahibzada M (2000) Solid State Ionics 134:103
30. Steele BCH (2000) Solid State Ionics 129:95

31. Wang S, Lu X, Liu M (2002) J Solid State Electrochem 6:95
32. Wang S, KatoT, Nagata S, Honda T, Kaneko T, Ivasita N, Dokiya M (2002) Solid State Ionics 146:203
33. Ullmann H, Trofimenko N (1999) Solid State Ionics 119:1
34. Kharton VV, Yaremchenko AA, Naumovich EN (1999) J Solid State Electrochem 3:303
35. Kim J-W, Virkar AV, Fung K-Z, Metha K, Singhal SC (1999) J Electrochem Soc 146:69
36. MacDonald RJ, ZView for Windows (Version 2.7). Scribner, Southern Pines, NC, USA
37. MacDonald JR (ed) (1987) Impedance spectroscopy: emphasisizing solid materials and systems. Wiley, New York
38. Sluyters-Rehbach M, Sluyters J (1970) In: Bard A (ed) Electroanalytical chemistry, vol 4. Macel Dekker, New York, p 76
39. Lasia A (1999) In: Conway BE, Bockris J O'M, White RE (eds) Modern aspects of electrochemistry, vol 32. Kluwer/Plenum, New York, p 143
40. Gabrielli C (1995) In: Rubinstein I (ed) Physical electrochemistry—principles, methods and application. Marcel Dekker, New York, p 257
41. Jacobsen T, West K (1992) Electrochim Acta 40:233
42. Bisquert J, Garcia-Belmonte G, Fabregat-Santiago F, Bueno RR (1999) J Electroanal Chem 475:152
43. Bisquert J, Compte A (2001) J Electroanal Chem 499:112
44. Chan SH, Chen XJ, Khor KA (2004) J Electrochem Soc 151:A164
45. van Heuveln FH, Bouwmeester HJM (1997) J Electrochem Soc 144:134